A&A 465, 1061–1067 (2007)
DOI: 10.1051/0004-6361:20065534

Astronomy & Astrophysics

Behavior of Comet 9P/Tempel 1 around the Deep Impact event

L. M. Lara[1], H. Boehnhardt[2], R. Gredel[3], P. J. Gutiérrez[1], R. Rodrigo[1], and M. J. Vidal-Nuñez[1]

[1] Instituto de Astrofísica de Andalucía, CSIC, PO Box 3004, 18080 Granada, Spain
e-mail: lara@iaa.es
[2] Max-Planck Institut für Sonnensystemforschung, Max-Planck-Str. 2, 37191 Katlenburg-Lindau, Germany
e-mail: boehnhardt@mps.mpg.de
[3] Max-Planck Institut für Astronomie, Königstuhl 17, 69117 Heidelberg, Germany
e-mail: gredel@caha.es

Received 3 May 2006 / Accepted 15 December 2006

ABSTRACT

Context. Comet 9P/Tempel 1, the target of the Deep Impact (DI) Mission, has been monitored from June 18 until July 12, 2005, as a follow up to the long-term campaign started in Jan. 2005.
Aims. The goal of this campaign is to characterize the comet before the DI event and to detect changes in activity and coma morphology produced by the DI experiment on July 04.226 UT 2005.
Methods. Optical broadband images and long-slit spectroscopic measurements have been acquired with the instrument CAFOS mounted at the 2.2 m telescope at Calar Alto Observatory (CSIC-MPG) from July 1 to 11, whereas only imaging has been performed with Versarray at the 1.5 m telescope of the Sierra Nevada Observatory (IAA-CSIC) on June 26 and 29, 2005.
Results. Fifteen hours after the impact, the ejecta cloud extends over ∼240° in position angle (PA) with a symmetry axis at PA ∼ 235°. The effect of the solar radiation pressure is already visible as a slight deviation from a fully symmetric plume and the ejecta dust is already feeding the tail. The exhaustive analysis of the broadband images has revealed that no new long-lasting coma structure is produced by the impact. The structures existing in the coma before the event are recovered after the ejecta plume has moved out. The maximum projected expansion velocity of the ejecta dust results in ∼230 and ∼150 m/s 15 and 40 h after impact, respectively. Surface brightness profiles of the continuum, either azimuthally averaged profiles from the broadband images or in the north-south direction from the long-slit spectra can generally be well fit with a slope m of $-0.94 \leq m \leq -1.49$ in $\log B - \log \rho$ representation. A few exceptions occur on July 2 and 8−10 when much flatter continuum profiles are detected that are possibly related to fragmentation processes and to the reported outbursts occurring around those dates. Normalized color S' of the dust inside the coma does not show spatial variations excluding July 04.875 UT, our first observation after the impact. At that time, the dust inside the ejecta plume is undoubtedly bluer than the surrounding coma ($8.2 \pm 0.4\%/100$ nm versus $14.5 \pm 0.8\%/100$ nm). The dust color averaged at $\rho \leq 10\,000$ km returns to a ∼12%/100 nm on July 07.875 UT, the same value measured a few days before the projectile impact. A lower limit to the mass in the ejecta can be given from our optical observations resulting in 1.2×10^6 kg, which represents about 14 h of quiet (i.e., steady state) pre-impact activity. The value of $Af\rho$ is remarkably variable during the 18 days monitoring as several outbursts took place, beside the one induced by the DI experiment. Apart from outburst periods, $Af\rho \sim 110$−120 cm. The gas activity represented by the CN, C_2, and C_3 production rates (Q), are relatively constant from July 1 to 6 excluding the immediate post-impact period on July 4. The number of molecules of CN, C_2, and C_3 produced by the DI were equal to 2.13×10^{29}, 2.07×10^{29}, and 1.49×10^{28} as measured 15 hrs after impact. The amount of their potential parent species detected at other wavelengths seems to indicate that a large fraction of the daughter species measured 15 h after the impact might originate from the ejected dust grains.
Conclusions. General conclusions include (i) new post-impact refractory material different from that seen pre-impact was ejected during the DI experiment, i.e., these dust grains had either different optical properties or a size distribution peaking at smaller sizes, (ii) the DI event did not initiate a long-lasting period of sustained cometary activity, and (iii) in many ways the artificial impact looked very much like a natural outburst of the comet, also (iv) some fraction of gaseous daughter species within the coma after the DI experiment might have originated in the ejected dust grains.

Key words. comets: individual: 9P/Tempel 1

1. Introduction

On July 4, 2005, the impactor of NASA's Deep Impact mission hit the surface of comet 9P/Tempel 1 with a relative velocity of 10.3 km s^{-1}. The collision of the impactor with a mass of 362 kg was expected to generate a crater (predicted diameter ∼100−125 m, A'Hearn et al. 2005a) and to eject cometary material into the coma. The Deep Impact (DI hereafter) mission was designed to have much of the mission-critical science done from Earth-based telescopes, and an overview of the scientific conclusions and collective observations from the world-wide campaign has been presented by Meech et al. (2005). As the most outstanding results, it is worth mentioning that new post-impact material with a different composition from that seen pre-impact was ejected, that the dust-to-gas mass ratio in the ejecta was much larger than pre-impact, and that the new activity was not detected for longer than a few days. As seen from ground, the DI event did not initiate a long-lasting period of sustained cometary activity, and in many ways the artificial impact looked very much like a natural outburst of the comet. However, the observations revealed some changes in the properties and behavior of the gas and dust at the impact and during the post-impact phase.

The search for parent volatiles between 2.8 and 5.0 μm by Mumma et al. (2005) resulted in the detection of eight species.

The abundance relative to water after the impact did not change for the CH_3OH and HCN molecules, whereas ethane was two times more abundant after than before the impact. Mumma et al. (2005) conclude that abundance ratios in the ejecta are similar to those of most Oort Cloud comets, but methanol and acetylene are lower in Tempel 1 by a factor of 2.

The study of the dust component by Sugita et al. (2005) and by Harker et al. (2005) indicates that the large-scale dust plume ejected by the impact contained a mass of $\sim 10^4$–10^6 kg of dust, depending on the model, and formed two wings at approximately ±45° from the symmetric center at PA ∼ 235°. Grain properties derived from these IR observations at the time of the impact reveal the presence of crystalline silicates, and its ratio to amorphous silicates is rather close to that for Oort cloud comets as C/1995 O1 (Hale-Bopp) and C/2001 Q4 (NEAT). The grain size distribution seems to peak at 1 μm, although the dust likely ranged in size from <1 μm to ∼10 μm across, and perhaps even larger.

This event was also followed by the optical cameras OSIRIS on board the Rosetta (ESA) spacecraft (Keller et al. 2005; Küppers et al. 2005) which overall gave rise to similar conclusions to the ones obtained from ground-based observatories. These authors also concluded that the CN-to-H_2O production rate was slightly enhanced in the impact cloud compared to that of normal comet activity, that HCN was likely more important relative to other CN parents in the cometary nucleus than on the surface, that the dust particles were flowing outward in the coma at $v > 160$ m/s, accelerated by the gas and/or by water molecules sublimated by solar radiation, and that the dust-to-water mass ratio is much larger than 1. Before this event, the comet had been characterized by Lara et al. (2006) by means of a continuous optical monitoring of its activity, coma morphology and evolution from January to June 18, 2005. The observations and results we present here, are a continuation of this 6 months monitoring carried out from ground. They aim at studying the gas and approximate dust ($Af\rho$) production rates, and the coma morphology for about 3 weeks around the DI event.

2. Observations and data reduction

From June 18 to July 12, 2005, the comet was observed from the Calar Alto Observatory (CSIC-MPG, near Almería, Spain), and from the Sierra Nevada Observatory (CSIC, near Granada, Spain; during June only), as a follow-up to the monitoring of the comet started in January 2005. Instruments and their setup at both observatories were the same as the ones used for the long-term comet monitoring, that is, broadband images and long-slit spectrophotometric observations were acquired.

Imaging: We used the instrument CAFOS (2048 × 2048 pixels, pixel size: 0.″53, FOV 18′ × 18′) mounted at the 2.2 m telescope at Calar Alto. Only the 1 × 1 k central pixels were used. Thus, the FOV covered by our observations is 9′ × 9′, whereas from the 1.5 m telescope at Sierra Nevada Observatory (CSIC), the Versarray CCD camera (2048 × 2048 pixels, pixel size: 0.″232, with a 2 × 2 binning, FOV 7.′9 × 7.′9) was used. The comet was imaged with a Johnson *R* and *I* broadband filter. In each filter, consecutive series of 3 to 5 images were acquired. Appropriate bias and flat-field frames were also taken each night. If photometric conditions prevailed, photometric standard stars were observed at airmass similar to the comet.

Spectroscopy: The spectroscopic measurements were done using CAFOS with grism B200 for every date excluding July 09 and 10 when B400 was used (see `http://www.caha.es/alises/cafos/cafos22.pdf` for more details; observable spectral range between 3200 and 8800 Å with a wavelength scale of 4.75 Å per pixel, and between 2800 Å and 1.0 μm with a wavelength scale of 9.7 Å per pixel, respectively). The slit of the spectrograph was orientated in a north-south direction. For absolute calibration, observations of appropriate spectrophotometric standard stars were acquired.

All comet observations were done with telescope tracking at the comet's proper motion. The visitor mode at the Calar Alto Observatory (Consejo Superior de Investigaciones Científicas-Max Planck Gesellschaft, CSIC-MPG, near Almería, Spain) was preferred during the 1–12 July observations of the comet, otherwise the data were acquired in service mode at either observatory. Details of the observations are given in Table 1. For July 9 and 10, it has not been possible to flux-calibrate the spectroscopic measurements as the sky conditions considerably worsened at the time of the spectrum acquisition of the calibration star. The images and spectra were reduced and calibrated in the same way as in Lara et al. (2004, 2006), and they are not repeated here.

3. Data analysis and results

3.1. Gas

Gas profiles (emission flux and column density) for CN, C_2, and C_3 vs. projected cometocentric distance ρ have been derived from the spectroscopic observations between July 2 and 8, (excluding July 7 due to passing clouds). On July 9 and 10, sky conditions considerably worsened while acquiring the comet and standard star spectra.

Figure 1 shows the energy flux vs. ρ in the north-south direction (imposed by the fixed orientation of the slit) for July 3, 4, and 5. These radial profiles indicate intensity variations and asymmetries in the coma due to the impact. NH_2 is not clearly detected in our spectroscopic measurements, and thus its profile as well as production rate cannot be reliably derived.

CN is the species that suffered a more pronounced variation on July 4 compared to the previous and following days. Lara et al. (2006) reported a clear CN north-south asymmetry for every spectroscopic measurement of the comet since mid-April 2005 in their long-term pre-impact monitoring of the comet. The degree of asymmetry changed with time during the two intervals of nightly observations in April, and an approximate period of ∼4 days is tentatively determined. This same behavior, excluding that due to the DI event, has also been detected during the July run. These variations might be due to the presence of a CN jet whose emission cone, as projected on the plane of the sky, points to the southern coma hemisphere where the slit is positioned.

From the data and results presented in this work, the CN emission on July 4 is considerably more isotropic than before and after the DI event. On July 4, the CN emission is 4 times higher in north direction, whereas in south direction the enhancement is only by a factor of 2.5 relative to adjacent days in the coma region $10\,000 \leq \rho \leq 20\,000$ km resulting in a more isotropic CN coma than previously observed. On July 5, 40 h after impact, the persistent north-south CN asymmetry is again clearly detected.

For C_3 and C_2 the flux enhancement is only a factor ≤2, and no obvious asymmetry between the northern and southern coma hemisphere is seen either 15 h after the impact or during the 10 days the comet was monitored (note that coma asymmetry does not depend on flux calibration, which it was not possible to perform on July 9 and 10).

Table 1. Observations log and results.

Date	r_h	Δ	PA	$Af\rho$	Q (s^{-1}) N^a (mol.)			log Qs		
(UT)	(AU)	(AU)	(°)	(cm)	CN	C_2	C_3	C_2/CN	C_3/CN	$Af\rho$/CN
June 24.918	1.509	0.848	112.7	146.1						
June 26.875	1.509	0.857	112.4	114.2						
June 29.854	1.507	0.872	112.0	150.1						
July 1.917	1.506	0.882	111.7	130.4						
July 2.917	1.506	0.887	111.6	125.1	1.17×10^{25}	1.13×10^{25}	1.31×10^{24}	–0.015	–0.951	–22.97
					1.84×10^{29}	*1.35×10^{29}*	*1.18×10^{28}*			
July 3.917	1.506	0.892	111.4	128.0	1.07×10^{25}	1.04×10^{25}	9.79×10^{23}	–0.012	–1.039	–22.92
					1.85×10^{29}	*8.54×10^{28}*	*1.66×10^{28}*			
July 4.917	1.506	0.897	111.3	204.1	2.38×10^{25}	2.30×10^{25}	2.09×10^{24}	–0.015	–1.056	–23.07
					3.97×10^{29}	*3.17×10^{29}*	*2.91×10^{28}*			
July 5.917	1.506	0.902	111.1	162.1	1.44×10^{25}	1.45×10^{25}	1.41×10^{24}	0.003	–1.009	–22.95
					2.57×10^{29}	*1.06×10^{29}*	*1.60×10^{28}*			
July 6.917	1.506	0.908	111.0	123.4	1.12×10^{25}	1.12×10^{25}	7.26×10^{23}	0.000	–1.188	–22.96
					2.32×10^{29}	*1.34×10^{29}*	*1.77×10^{28}*			
July 7.917	1.506	0.913	110.9	120.4						
July 8.917	1.506	0.919	110.7	137.2	1.53×10^{25}	1.65×10^{25}	9.17×10^{23}	0.033	–1.222	–23.07
					3.68×10^{29}	*1.88×10^{29}*	*3.40×10^{28}*			
July 9.917	1.506	0.925	110.6	138.4						
July 10.917	1.506	0.930	110.5	140.1						
July 11.917	1.506	0.936	110.4	116.6						
July 12.917	1.506	0.942	110.2	121.4						

- Date (UT) refers to the mean value of the time interval at which the comet could be observed from Calar Alto (CSIC-MPG) from July 1 to 12. During June, as only one sequence of 3 or 5 images was acquired from either observatory, the date refers to the time of observations.
- r_h and Δ are the heliocentric and geocentric distances of the comet during our observations, respectively.
- PA refers to the position angle of the extended Sun−target radius vector counted north over east.
- [a] The total number of molecules, for each species, integrated in a circular aperture of 30 000 km projected radius at comet distance and centered on the nucleus position, radius is listed, in italics below the gas production rates, Q.
- Uncertainties in $Af\rho$ and Q are estimated to be ≤10% and ≤15%, respectively.

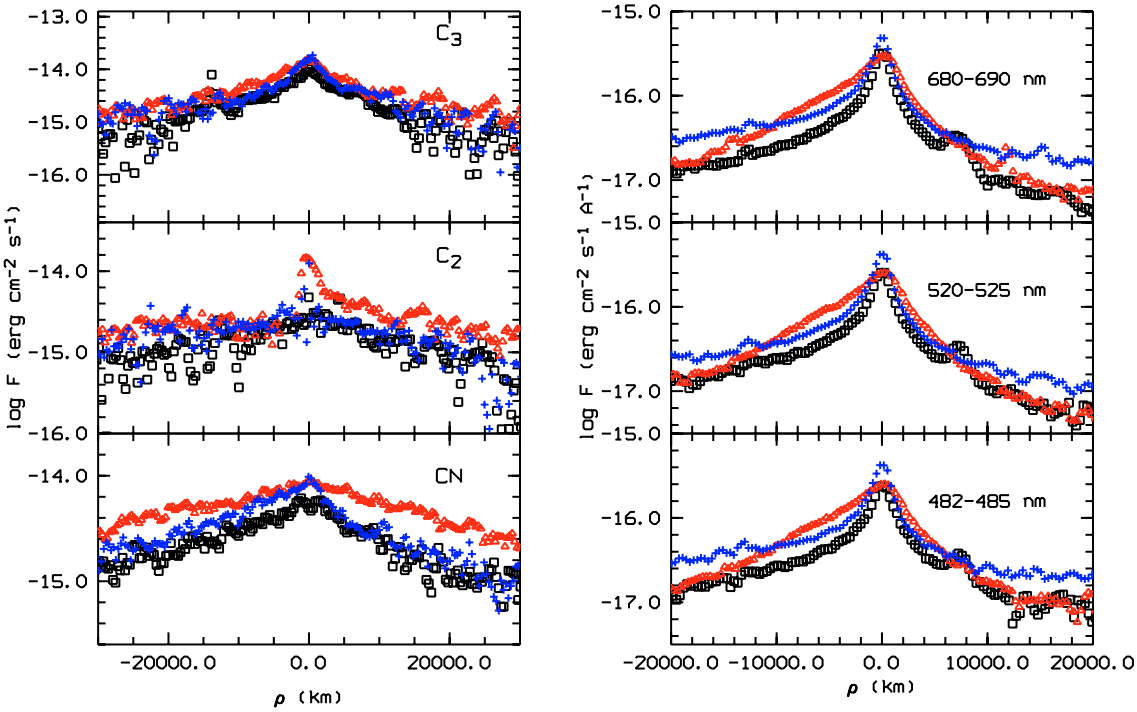

Fig. 1. *Left panel*: radial profiles of the C_3, C_2, and CN fluorescence emission in the north-south direction derived from the spectroscopic observations. Black squares refer to July 3, red triangles to July 4, and blue crosses to July 5. *Right panel*: comet flux measured in three clear continuum regions. The ejecta cloud at the time of our observations extended from position angles (PA) 125° (south-east direction) to 350° (north direction), whereas the slit was orientated in the north-south direction. The south direction is at $\rho \leq 0.0$ and the north direction at $\rho \geq 0.0$.

The conversion of the emission band fluxes into column densities uses constant g-factors for C_2 and C_3 (A'Hearn et al. 1995), whereas the g-factor of the CN molecule is calculated for each observing epoch according to Schleicher (1983). The gas production rates are obtained by means of the Haser (1957) modeling with customary $v_d = 1$ km s^{-1}, whereas $v_p = 0.86 r_h^{-0.4} = 0.703$ km s^{-1}. Scale lengths for every species are taken from A'Hearn et al. (1995). The resulting production rates are listed in Table 1. Our production rates for CN, Q_{CN}, for July 2 and 3 compare favorably with the ones for HCN as measured by Biver et al. (2005, private communication). Our mean value of 1.12×10^{25} s^{-1} for July 2.79−3.88 UT is well compatible with HCN being the dominant or even sole parent of CN in this comet assuming a parent scalelength, l_p, of 13 000 km. The HCN production rate reported from millimeter observations remains constant at the post-impact phase according to Biver et al. (2005, private communication), which is also the case – within the errors – for CN derived from our optical observations on July 5 and 6. For July 4 due to the impulsive event, a model to derive the production rates by assuming steady-state production of gas expanding isotropically (as assumed by the Haser model) is not applicable. Nonetheless, the Q listed Table 1 is included only as reference, and it should be interpreted solely as an indicator of the actual activity level.

A more rigorous approach is to estimate the number of molecules detected in the coma of Tempel 1 that arose from the DI collision. For that, we have measured the total number of molecules N_{tot} of the different species (CN, C_2, and C_3) in certain apertures to provide us with N_{tot} vs. ρ from an average spectrum obtained from those acquired on July 2 and 3 (as representative of steady-state conditions) and July 4 (after impact). We then subtracted the averaged profile $N_{tot}(\rho)$ of July 2 and 3 from that of July 4. This results in the total number of molecules produced by the DI collision. Hence, the number of daughter species, produced by the impact and measured in an aperture of radius $\rho = 30\,000$ km (beyond this projected distance the spectra are relatively noisy) about 15 h after the event, are 2.13×10^{29}, 2.07×10^{29}, and 1.52×10^{28}, respectively. These values of N_{tot} can be used to infer the number density of parent species that were produced by the DI event, at the time of the collision, in a similar way to that described by Küppers et al. (2005). For this computation, a parent lifetime τ_p must be considered. Assuming that $\tau_p = l_p/v_p$ is a good approximation and that $v_p = 0.703$ km s^{-1} represents the gas outflow velocity at the impact time, then $\tau_p = 18\,570$ s. Similarly, we assume that the daughter species are ejected from the parent photodissociation with $v_d = 1$ km s^{-1}, hence $\tau_d = 210\,000$ s. Hence, the impact produced 2.83×10^{29} molecules whose dissociation gave rise to CN with an efficiency of 1.0.

Bearing in mind the uncertainty in determining the CN parent molecule we have produced theoretical CN column density profiles vs. ρ for different $\tau_p = 18\,570$ s, 30 000 s, 55 000 s, and 70 000 s. The (significant) fit to the observed CN profiles on July 3, 4, and 5 is best for short parent lifetimes (18 570 and/or 30 000 s) on July 3 and 5, whereas on July 04, a better agreement between observations and theory is achieved by using longer parent lifetimes (55 000 and/or 70 000 s). This result is in line with that obtained by Küppers et al. (2005), that is, the CN produced by the impact is in better agreement with a long lifetime ($>4 \times 10^4$ s) of the CN parent species (such as, e.g., HCN).

Mumma et al. (2005) detected HCN in the post-impact phase measuring a total number of molecules of $\sim(1.81 \pm 0.18) \times 10^{28}$ within 1000 km from the comet nucleus at ∼2 h after impact. Our CN measurements were done 15 h after impact in a much larger circular aperture of 30 000 km. Although both measurements are not directly comparable (most likely the gas production rates were time dependent during and after the impact) and the apertures are quite different, it cannot be ruled out that the discrepancy between HCN and CN number density might be indicative of CN being largely produced in the ejecta cloud either by other gaseous parent species or by the icy dust grains.

The integrated number density of C_2 and C_3 precursors produced by the impact is 3.93×10^{29} and 1.06×10^{29}, for $\tau_p = 22\,000$ s and 2800 s, respectively. The parents of C_2 and C_3 are not known and indeed these daughter species might be produced by two- or three-step photodissociation processes. From the potential precursors of C_2, ethane (C_2H_6) and acetylene (C_2H_2) were both seen during the post-impact phase by Mumma et al. (2005). The total number of ethane and acetylene molecules reported by these authors is (4.56×10^{28} vs. 1.80×10^{29}). As in the case of HCN and CN, this amount is too low to account for the number of C_2 molecules produced by the impact that we have detected in our observations 15 h after it happened. However, as previously mentioned, the comparison is not straightforward and this discrepancy must be regarded with caution.

The abundance of every species relative to CN remains rather stable during the monitoring reported here. This stability applies in particular for July 4 and 5, i.e., 15 and 40 h (or one rotation) after impact. The quantities Q_{C_2}/Q_{CN} and Q_{C_3}/Q_{CN} can be considered as constant over the period the comet has been monitored, and the comet 9P can be regarded as typical regarding C_2 within the taxonomical classification established by A'Hearn et al. (1995). The values of the C_3 production rate presented here are in agreement with the results in Boehnhardt et al. (2006), as well as the ratios log (C_3/CN) and log (C_2/CN), whereas considerable discrepancies appear when comparing Q_{C_3} presented by Schleicher et al. (2006) and our results.

Table 1 also provides evidence that the comet experienced increased activity on July 8, and that its evolution could not be monitored for the following days. At the time this outburst occurred, beside the broadband imaging of the comet, our spectroscopic measurements indicate a clear enhancement of the gas production rates of daughter species in the optical wavelength range. This behavior has not been assessed in any of the previous reported outbursts as there were no simultaneous imaging and spectroscopic observations of the comet.

3.2. Dust

The study of dust properties and dynamics is done from the broadband images (R and I Johnson filters), as well as from the long-slit spectra. The images show – after computer processing as described in Lara et al. (2006) (i.e., adaptive Laplace filtering (Boehnhardt & Birkle 1994; Boehnhardt et al. 1999) and radial renormalization (A'Hearn et al. 1986) – the geometry of dust structures in the cometary coma. Figure 2 provides a view of the temporal evolution of the coma structures from June 26 to July 5, 2005. Before the impact, the only existing structures are those already reported by Lara et al. (2006), whereas ∼15 h and 40 h after the impact the dust cloud produced by the DI experiment is clearly seen, as well as its expansion in the southwest direction. At that time, the coma structures existing before the impact are mostly hidden by the ejecta plume. However, they became clearly visible again when the ejecta cloud had expanded and attenuated over the following days. By dividing the images obtained on July 4 and 5 by those on July 3, the expansion

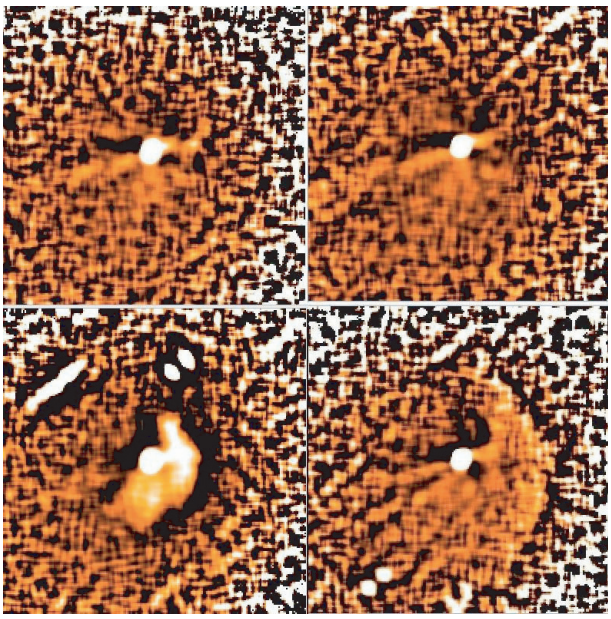

Fig. 2. Laplace-filtered images of the coma structures of comet 9P/Tempel 1 as imaged in the *R* Johnson filter on June 26 and 29, and July 4 and 5, from top left to bottom right. North is up and east to the left. The field of view is 60 000 × 60 000 km and the nucleus is at the center of the FOV. On June 26 and 29, a linear structure appeared in approximately the east-west direction. Other fainter structures can be seen in the southern hemisphere. On July 4, ∼15 h after the impact, the dust cloud produced by the Deep Impact experiment is clearly seen. The leading edge of the cloud ejecta extends up to ∼13 000 km in position angles 125° to 350°. Forty hours after impact, i.e., July 5, the expanding dust cloud forms a shell that has noticeably changed shape due to the push of the solar radiation pressure forcing the particles into the tail. It reaches $\rho \sim 23\,000$ km in the sunward direction (the PA of the Sun is ∼297° counted north over east).

velocity, projected on the plane of the sky at PA = 235 ± 20°, of the leading edge of the ejecta cloud can be computed giving rise ∼230 m/s and ∼152 m/s, 15 and 40 h after impact.

The ejecta cloud is still visible in our Calar Alto images of July 6. It has noticeably changed shape due to the solar radiation pressure pushing the particles into tail direction. No new long-lived jet or fan, as a consequence of the impact crater, is detected either in our Calar Alto images or reported from other observations around the world (to our knowledge). Signatures of the ejecta cloud were still seen in imaging observations on July 7 (Meech et al. 2005)

The study of the angular profile of the dust plume provided information on the DI cratering process and the subsequent plume dynamics (see Sugita et al. 2005). This plume dynamics can be further monitored from our images 15 h after the impact. Figure 3 shows angular profiles of the surface brightness of the dust plume at different radial distances from the nucleus. These profiles have been computed from a fully $Af\rho^2 (\approx F_c/F_{\rm Sun})$ calibrated *R* Johnson image on July 4 subtracted by the one on July 3, such that only the surface brightness due to the ejecta produced by the DI collision remains in the resulting image as in Fig. 4. This approach assumes that the overall activity of the nucleus (i.e., except that caused by DI) is steady state and at the same level as on July 3.

An anisotropic brightness distribution can be seen at every position angle (PA) and at every projected cometocentric distance. Near the leading edge of the dust plume ($\rho \sim 12\,000$ km), the angular brightness profile may still reflect the presence of a classic eject curtain (peaks in about a ±45° direction from the symmetric center) as described by Sugita et al. (2005), although its shape is considerably distorted due to the Sun radiation pressure that is pushing the dust grains into the tail in an approximately south-east direction, i.e., PA ∼ 160°. Another feature worth to mentioning is the peak at 12 000 km and PA ∼ 340−350° with a width of about 25°, whose enhanced brightness pertains to the ejected material in that direction (see Fig. 2) at the impact and which, 15 h after impact, had still not been still distorted by the solar radiation pressure. In the inner coma, at 1000−3000 km and PA ∼ 100−360°, the brightness is as much as a factor of 6 higher in an opening angle of ∼230° centered at ∼235°, the symmetric center of the plume, than at other angular positions.

The continuum surface brightness profiles B vs. ρ have been derived from the spectra as well, in regions free from gas contamination. For almost every day, these profiles can be linearly fitted in log − log representation, with the slope parameters $-0.85 \leq m \leq -1.49$. Some exceptions occur on July 2 in the south direction ($m \approx -0.50$) and on July 5 to 8 in both the north and south directions (much flatter radial profile $-0.43 \leq m \leq -0.94$). This non-canonical behavior of log B vs. log ρ is also obtained from the *R* Johnson broadband images when extracting cuts by means of an imaginary slit of 2″ width in N-S direction. The flatter slopes in the profiles might be due to grain fragmentation.

Dust color maps have been computed as the normalized reflectivity gradient S' in %/100 nm defined as

$$S' = \frac{2}{S_I + S_R}\left(\frac{S_I - S_R}{\lambda_I - \lambda_R}\right), \quad (1)$$

where S is the cometary flux measured in the bandpass of each filter divided by the Sun flux in the same bandpass, I refers to the *I* Johnson filter centered at 850 nm and R to the *R* Johnson filter centered at 641 nm. On every date, these maps do not show variations of the grain properties (size and/or composition) in the coma of 9P/Tempel 1 in the inner coma, excluding July 4. At about fifteen hours after the impact, the dust color within the ejecta plume is bluer than in the rest of the coma up to projected distances of $\rho \sim 15\,000$ km. However, on July 5, 40 h after impact, the dust coma shows a weak trend toward an overall blueing at $\rho \leq 15\,000$ km (see Table 2), whereas on July 7, S' returns to value in the order of 10%/100 nm. Figures 5 and 6 display the dust color variations in 2D and in selected cuts in north-south, east-west directions and through the ejecta plume, respectively. It can be seen that the reflectivity gradient is lower (∼6−8%/100 nm vs. ∼14−16%/100 nm) in those directions that are populated by the grains ejected by the impact, i.e., the dust color is bluer than in adjacent regions, meaning that either there is an overpopulation of submicrometer to micrometer dust grains (as it has been widely reported by Sugita et al. 2005; Harker et al. 2005; A'Hearn et al. 2005b; and Meech et al. 2005 from observations in the mid-IR) or they are more refractive in the blue range than in the red. This same behavior can be seen in our spectra when selecting spectral regions well known to be free from gas contamination. Beside these dust color variations in the coma of 9P/Tempel 1, around fifteen hours after the impact, the considerable asymmetry in the north-south and east-west directions on July 4 (see Fig. 6) is not seen either on July 3 or on July 5. Table 2 lists the average dust color in the coma region $2000 \leq \rho \leq 10\,000$ km in the north and south directions on July 3 through 5. Beyond ∼15 000 km up to ∼32 000 km, the mean dust normalized reflectivity is ∼16%/100 nm in the south (approximately tail) direction with a trend of $S' \sim 20\%/100$ nm, whereas

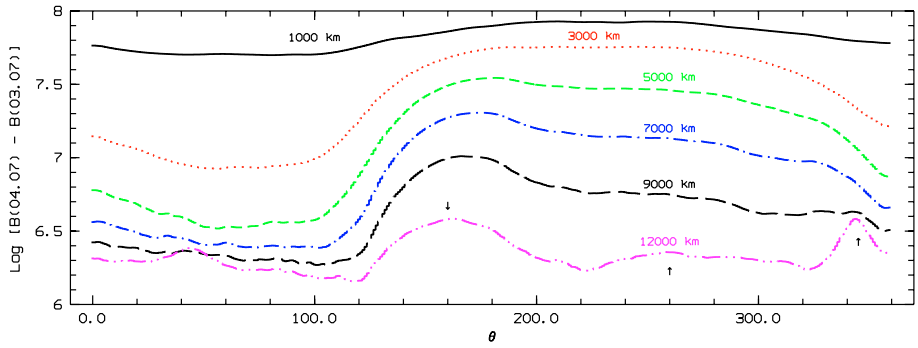

Fig. 3. Angular profiles of surface brightness, B, of 9P/Tempel 1 15 h after impact obtained as a difference of B on July 3 and 4. The log of the surface brightness is shown as a function of azimuth θ at several distances from the nucleus. North corresponds to $\theta = 0°$ and east to $\theta = 90°$. The symmetric center of the dust plume is ~235° and it extends for ~240°. The three vertical arrows shows the most prominent features at the outer coma at position angles of ~160°, the displaced center of the plume at ~260°, and a relatively narrow increase of B centered at ~345° and width of ~25°.

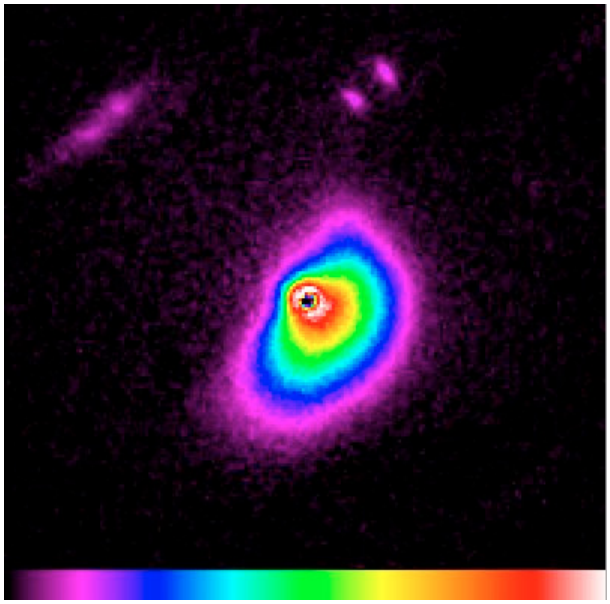

Fig. 4. Two-dimensional image of the dust plume surface brightness. It has been computed as the difference between the image of 9P/Tempel 1 on July 4, calibrated in $Af\rho^2$ (proportional to $\frac{F_{\rm comet}}{F_{\rm Sun}}$), and the one on July 03. The field of view is 60 000 × 60 000 km at the comet distance. North is up, east to the left. The look-up table is linear and it stretches from 10^6 to 10^8 cm^2.

at any other direction the measurements scatter too widely to derive a reliable result for the dust reddening.

The approximate dust production rate of 9P/Tempel 1 was monitored from June 24 to July 12. Beside the increase in $Af\rho$ produced by the DI experiment on July 4 (whose aftermath was still measurable on July 5), we note some sporadic increases in the dust production rate on June 24 and 29 (likely connected to a natural outburst reported in mid-IR (Wooden et al. private communication) observations that increased the comet brightness by ~20%. In a very approximate way, the $Af\rho$ measured on July 4 can be used to estimate the total mass of dust produced by the impact itself. For this, we have subtracted the $Af\rho$ value measured on July 4 in an aperture of 5000 km from the one on July 3 (again assuming steady state general dust production rate for 9P/Tempel 1). This gives rise to $Af\rho_{\rm impact} = 76$ cm, which for a typical dust albedo of 0.01, grain size of 1 micron, and density of 1 gr/cm^3 gives rise to ~1.2×10^6 kg of dust liberated by the impact, the equivalent of ~14.5 h of pre-impact regular activity (i.e., about $Q_{\rm dust} \approx 23$ kg/s in steady-state conditions, radial outflow of the long-lived grains with the same physical properties as mentioned above).

Table 2. Spatially averaged (2000 km ≤ ρ ≤ 10 000 km) dust reddening in units of %/100 nm within the coma of 9P/Tempel 1 around the impact event.

Direction[a]	Date		
	July 03	July 04	July 05
North	11.03 ± 1.8	15.04 ± 0.9	9.9 ± 1.6
South	9.9 ± 1.1	8.6 ± 0.8	8.5 ± 0.6
East	10.6 ± 1.4	13.6 ± 0.7	9.4 ± 1.9
West	9.8 ± 3.3	8.07 ± 1.4	8.2 ± 1.8
PA ~ 235°	10.5 ± 1.3	7.9 ± 1.08	8.04 ± 1.9
PA ~ 45°	9.5 ± 0.7	14.8 ± 0.7	8.2 ± 1.3

[a] Cuts along the different listed directions are obtained by means of an imaginary slit of 2″ width centered where the comet nucleus presumably is.
Errors in the normalized reflectivity are the standard deviation from the spatial average in the range 2000 ≤ ρ ≤ 10 000 km.

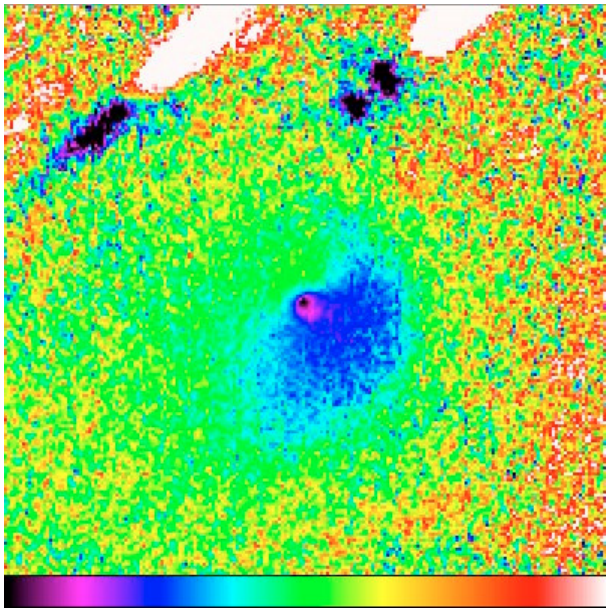

Fig. 5. Two-dimensional color map of the dust in the coma of 9P/Tempel 1 on July 4, i.e., ~15 h after impact. North is up and east to the left. The look-up table is linear between 0 and 30%. The field of view is 60 000×60 000 km at the comet distance centered at the nucleus.

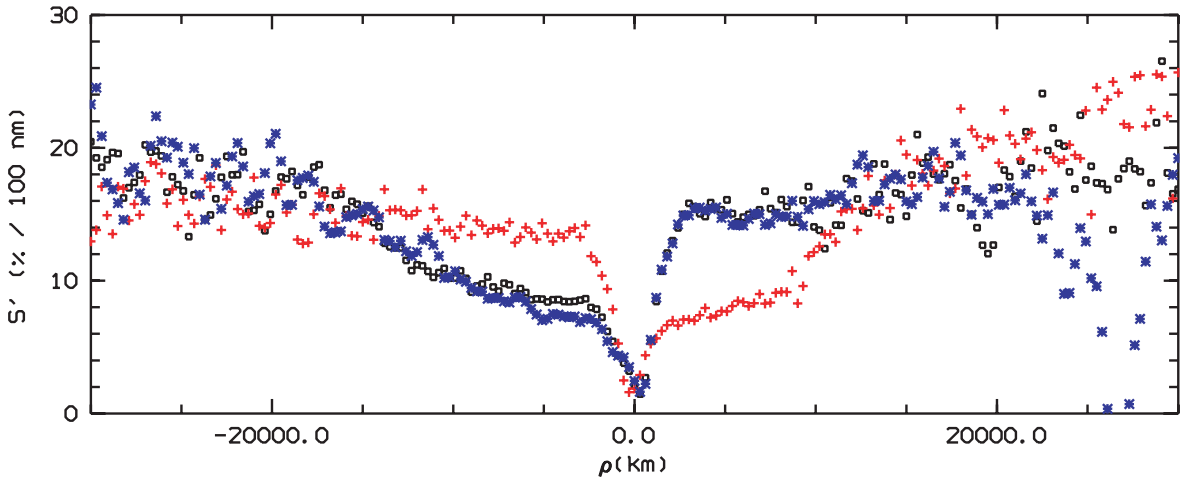

Fig. 6. Normalized reflectivity, or "continuum color" of the dust measured from the broadband *R* and *I* Johnson images on July 4 extracting cuts by means of an imaginary slit of 2″ width along different directions. Black dots: dust grain color in the north ($\rho > 0$) – south. Red crosses: west ($\rho > 0$) – east direction. Blue asterisks: across the dust cloud in the SW ($\rho > 0$) – NE ($\rho < 0$) direction. Note that the dust ejecta are placed in the SW direction.

4. Conclusions

The monitoring of 9P/Tempel 1 started on January 2005, whose results up to June 18 have been presented by Lara et al. (2006), was continued until July 12 to complete the scientific objectives of the project. The results presented here aim at a characterization of the comet behavior as approaching the time at which the DI s/c successfully delivered a projectile to impact the nucleus and the relatively long-term (i.e., ∼5 rotational periods) effects this experiment might have caused to the comet activity.

Beside the outburst induced by the DI experiment, the comet has shown to be rather variable in dust activity, as measured by means of the $Af\rho$ parameter. The dust activity induced by the DI experiment represents a ∼60% (computed from $Af\rho$ in Table 1) of the pre-impact activity monitored for a few days before the DI experiment. In an approximate way, the amount of dust produced by the projectile represented about 14 h of "normal" (i.e., steady state) comet activity. Fourteen hours after the impact, the ejecta cloud extended over ∼240° in position angle (PA) with symmetry axis at PA ∼ 235°. Maximum expansion velocity (projected on the plane of the sky) of the dust in the cloud was ∼230 m/s, very similar to the expansion velocity reported for natural outbursts. The dust populating this plume showed a lower reddening (gradient of the normalized reflectivity S' measured in %/100 nm) than the surrounding coma, pointing to the fact that either there was an overabundance of small dust particles within the ejecta plume, or dust particles ejected by the impactor were more refractive in the blue range than in the red one.

In a general way, the DI experiment did produced a noticeable increase of the gas activity, at least as derived from the optical observations acquired on July 04.917 UT that monitor the production rate of daughter species such as CN, C_2, and C_3. The total number of molecules of these daughter species produced by the impact represents a factor of 1.53, 3.56, and 7.47 the number of molecules measured inside a circular aperture of 30 000 km as produced by the steady activity of the comet. Additionally, there are indications that some of the dust expelled by the impact was partially responsible for the abundance of some of the molecules previously mentioned. This is particularly true for CN and C_2. Potential gaseous parent species were detected at the impact itself at other wavelength ranges, although their production rate during and following the impact could have been highly variable, the production rates of these parent species at the impact cannot account for the abundances of daughter species measured in the coma of 9P/Tempel 1 at about fifteen hours after the impact.

Our comet monitoring, which spanned almost 5 nucleus rotations, did not reveal any new long-lasting structure in the coma as a consequence of the impact. Further data until mid-August still remain to be analyzed and the results will be presented in a forthcoming paper. A first quick look at the images does not show coma structures in addition to the ones existing before the DI experiment.

Acknowledgements. Based on observations collected at the Centro Astronómico Hispano Alemán (CAHA) at Calar Alto, operated jointly by the Max-Planck Institut für Astronomie and the Instituto de Astrofísica de Andalucía (CSIC), and at the Sierra Nevada Observatory operated by the Instituto de Astrofísica de Andalucía (CSIC). We are grateful to the service observers J. Aceituno, A. Aguirre, M. Alises, N. Cardiel, V. Casanova, A. Guijarro, F. Hoyo, S. Pedraz, S. Sánchez, A. Sota, and U. Thiele at both observatories; without their engagement and dedication this program would not have been successful. The research carried out has been partially supported by the Spanish Ministerio de Ciencia y Tecnología under contracts ESP2003–0357. P.J. Gutiérrez acknowledges the support by a Juan de la Cierva contract.

References

A'Hearn, M. F., Hoban, S., Birch, P. V., et al. 1986, Nature, 324, 649
A'Hearn, M. F., Belton, M. J., Delamere, A., & Blume, W. H. 2005a, Space Sci. Rev., 117, 1
A'Hearn, M. F., Belton, M. J. S., Delamere, W. A., et al. 2005b, Science, 310, 258
A'Hearn, M. F., Millis, R. L. Schleicher, et al. 1995, Icarus, 118, 223
Boehnhardt, H., & Birkle, K. 1994, A&AS, 107, 101
Boehnhardt, H., Birkle, K., Fiedler, A., et al. 1999, EMP, 78, 179
Boehnhardt, H., et al. 2006, A&A, submitted
Harker, D. E., Woodward, C. E., & Wooden, D. H. 2005, Science, 310, 278
Haser, L. 1957, Bull. Cl. Sci. Acad. R. Belg., 43, 740
Keller, H. U., Jorda, L., Küppers, M., et al. 2005, Science, 310, 281
Küppers, M., Bertini, I., Fornasier, S., et al. 2005, Nature, 437, 987
Lara, L. M., Rodrigo, R., Tozzi, G. P., Boehnhardt, H., & Leisy, P. 2004, A&A, 423, 1169
Lara, L. M., Boehnhardt, H., Gredel, R., et al. 2006, A&A, 445, 1151
Meech, K. J., Ageorges, N., A'Hearn, M. F., et al. 2005, Science, 310, 265
Mumma, M., Di Santi, M. A., Magee-Sauer, K., et al. 2005, Science, 310, 270
Sugita, S., Ootsubo, T., Kadono, T., et al. 2005, Science, 310, 274
Schleicher, D. G. 1983, Ph.D. Dissertation, Univ. of Maryland
Schleicher, D. G., Barnes, K. L., & Baugh, N. F. 2006, AJ, 121, 1130.